DESY 17-090

# A New Approach to the BFKL Mechanism: Application to High-Precision HERA Data.



H. Kowalski [1], L.N. Lipatov [2], D.A. Ross [3], O. Schulz [4]

[1] *Deutsches Elektronen-Synchrotron DESY, D-22607 Hamburg, Germany*

[2] *St.Petersburg State University, St. Petersburg 199034 and Petersburg Nuclear Physics Institute, Gatchina 188300, Russia*

[3] *School of Physics and Astronomy, University of Southampton, Highfield, Southampton SO17 1BJ, UK*

[4] *Max Planck Institute for Physics, Munich, Germany*

**Abstract**

We analyse here in NLO the physical properties of the discrete eigenvalue solution for the BFKL equation. We show that a set of positive $\omega$ eigenfunctions together with a small contribution from a continuum of negative $\omega$'s provide an excellent description of high-precision HERA $F_2$ data in the region, $x < 0.001$, $Q^2 > 6$ GeV$^2$. The phases of the eigenfunctions can be obtained from a simple parametrisation of the pomeron spectrum, which has a natural motivation within BFKL. The data analysis shows that the first eigenfunction decouples or nearly decouples from the proton. This suggests that there exist an additional ground state, which has no nodes.

July 2017

# 1 Introduction

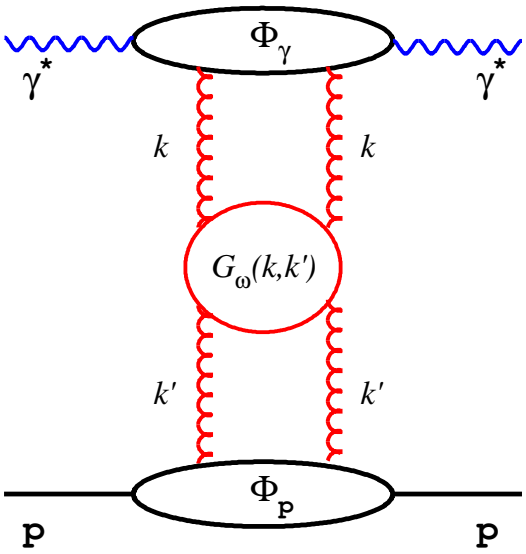


Figure 1: Evaluation of $F_2$ in $\gamma^*$ p scattering using the BFKL Green Function

The aim of this paper is to find a boundary condition which provides a precise description of HERA $F_2$ data using the BFKL Green Function approach developed in our two previous papers [1, 2]. In the search for this condition we were guided by the principle of simplicity and some analogy to the Balmer series. In the QCD version of the Regge theory developed here the BFKL equation is considered to be analogous to the Schrödinger equation for the wavefunction of the pomeron. The BFKL kernel corresponds to the Hamiltonian and the eigenvalues $\omega$ to the energy eigenvalues. Thus, we will specify this boundary condition in terms of a relation between the eigenvalues $\omega_n$ of the BFKL equation and the principal quantum number $n$. This relation determines then the boundary condition in terms of the phases $\eta_n$ of the eigenfunctions close to the non-perturbative region, $k \sim \Lambda_{\rm QCD}$.

The Green Function approach considered here is very suitable since it does not require any cutoff on the BFKL dynamics and provides a direct relation to the measurements at low-$x$. Thus, the deep inelastic structure function $F_2(x, Q^2)$ can be directly calculated as a convolution of the Green function with impact factors that encode the coupling of the Green function to the external particles that participate in that process.

$$F_2(x, Q^2) \;=\; \int dt dt' \Phi_\gamma(Q^2, t) \mathcal{G}(t, t', Y) \Phi_P(t'), \tag{1.1}$$

where, $Y = \ln(1/x)$, $t = \ln(k^2/\Lambda^2_{QCD})$, $t' = \ln(k'^2/\Lambda^2_{QCD})$; $k$, $k'$ being the transverse momenta of the gluons entering the BFKL amplitude. $\Phi_{DIS}(Q^2, t)$ describes the (perturbativly

calculable) coupling of the gluon with transverse momentum $k$ to a photon of virtuality $Q^2$ and $\Phi_P(t')$ describes the coupling of a gluon of transverse momentum $k'$ to the target proton, see Fig.1. [1]

The Green Function, defined by (2.3), is directly related to the gluon density (4.2), in the low $x$ region. The properties of this gluon density are very interesting to the LHC and cosmic ray physics. They are also interesting by themselves, because in difference to the DGLAP evolution [13], the BFKL equation describes a system of quasi-bound self-interacting gluons. Such a system is sensitive to confinement effects and has also some sensitivity to Super-Symmetry effects in the gluon sector, as was first observed in ref. [4, 5].

The paper is organised as follows: In Section 2 we recall the main properties of the BFKL Green Function and of their eigenfunctions, determined in our last papers [1, 2]. In Section 3 we introduce the NLO corrections to BFKL and evaluate the properties of eigenvalues and eigenfunctions in NLO. In Section 4 we apply this formalism to HERA data and describe the search for a proper boundary condition and its results. Finally, in Section 5 we summarise the results and conclude.

# 2 BFKL Green Function

In [1] we determined the BFKL Green Function $\mathcal{G}_\omega(t,t')$ (in Mellin space) from the equation

$$\left(\omega - \hat{\Omega}(t,\hat{\nu})\right)\mathcal{G}_\omega(t,t') \;=\; \delta(t-t'), \tag{2.1}$$

where $\hat{\Omega}$ denotes the BFKL operator, which was given in terms of the LO characteristic function, $\chi(\alpha_s(t),\nu)$, by

$$\hat{\Omega} \;=\; \sqrt{\bar{\alpha_s}(t)}\left(2\Psi(1) - \Psi\left(\frac{1}{2}+\frac{\partial}{\partial t}\right) - \Psi\left(\frac{1}{2}-\frac{\partial}{\partial t}\right)\right)\sqrt{\bar{\alpha_s}(t)}, \tag{2.2}$$

with $\bar{\alpha_s} \equiv C_A\alpha_s/\pi$. By placing $\sqrt{\bar{\alpha_s}(t)}$ on either side of the differential operator we assured the hermiticity of the whole operator.

We have shown in [1, 2] that the Green Function determined in this way has poles on the positive real axis of the $\omega$ plane and a cut along the negative $\omega$ axis. Therefore it can be constructed from the complete set of eigenfunctions of the BFKL operator in the usual way

$$\mathcal{G}(t,t',Y) \;=\; \sum_{n=1}^{\infty} x^{-\omega_n} f_{\omega_n}((t) f^*_{\omega_n}(t') + \lim_{\omega_{min}\to-\infty}\int_{\omega_{min}}^{0} d\omega x^{-\omega} f_{-|\omega|}(t) f_{-|\omega|}(t'). \tag{2.3}$$

The spectrum of the eigenvalues $\omega_n$ was found to be discrete for positive values of $\omega$ and continuous for negative value of $\omega$. The complete set of eigenfunctions with positive and negative eigenvalues $\omega$ was found to satisfy the closure relation and the orthonormality condition. In addition, the Green Function was quickly converging so it was sufficient to use only O(10) discrete eigenfunctions to describe properly the gluon density, as compared to our previous work [1], where we had to use more than 100 eigenfunctions.

[1] The variable $t$ is more appropriate for theoretical analysis, whereas $k$ is more appropriate for comparison with data.

## 2.1 Eigenvalues and eigenfunctions

In LO BFKL [14], with the fixed QCD coupling constant $\alpha_S$, the eigenfunctions have a simple oscillatory behaviour in terms of the gluon transverse variable $t$,

$$f_\omega(k) \;\sim\; \exp(\pm i\nu t), \tag{2.4}$$

The frequency $\nu$ of these oscillations is connected to the eigenvalue $\omega$ by the characteristic equation

$$\omega \;= \alpha_S\, \chi_0(\nu), \tag{2.5}$$

with

$$\chi_0(\nu) \;\equiv\; 2\Psi(1) - \Psi\left(\frac{1}{2} + i\nu\right) - \Psi\left(\frac{1}{2} - i\nu\right). \tag{2.6}$$

With fixed $\alpha_S$ the frequency $\nu$ is a one-to-one function of $\omega$. However, when $\alpha_S$ is running $\nu$ becomes a function of $t$, $\nu_\omega(t)$, in order to compensate the $t$ variation of $\alpha_S$. For sufficiently large values of $t$ there is no more a real solution for $\nu_\omega(t)$ of eq. 2.5. The transition from the real to imaginary values of $\nu_\omega(t)$ singles out a special value of $t = t_c$ for which

$$\nu_\omega(t_c) = 0. \tag{2.7}$$

For $t$ values below the critical point $t_c$ the behaviour of the eigenfunction stays oscillatory, but above it becomes exponentially suppressed. This fixes the phase of the eigenfunction at $t = t_c$ and together with some fixed non-perturbative phase $\eta_{NP}$ leads to quantisation, i.e to a discrete set of eigenfunctions.

To analyse the behaviour of the BFKL equation in the neighbourhood of the turning point, $t_c$, it is convenient to define first two related variables, $s_\omega(t)$ and $z(t)$. The variable $s_\omega(t)$ gives the phase shift from the turning point $t_c$ to the point $t$ and corresponds to the argument of the wave function of eq. 2.4. It is defined as

$$s_\omega(t) \;=\; \int_t^{t_c} dt'\, \nu_\omega(t') \tag{2.8}$$

and the ($\omega$ dependent) variable $z(t)$ is defined as

$$z(t) = -\left(\frac{3}{2} s_\omega(t)\right)^{\frac{2}{3}}. \tag{2.9}$$

Using these variables we have shown in [1] that the BFKL operator, $\hat{\Omega}$, can be related to the "generalized Airy operator" as

$$\left(\omega - \hat{\Omega}\left(t, -i\frac{\partial}{\partial t}\right)\right) \;\approx\; \frac{1}{N_\omega(t)} \left(\dot{z} z - \frac{\partial}{\partial t} \frac{1}{\dot{z}} \frac{\partial}{\partial t}\right) \frac{1}{N_\omega(t)}. \tag{2.10}$$

In this derivation the diffusion approximation was used in the vicinity of the turning point and the semi-classical one far away from it. Using these approximations we have shown [1,2] that the most general solution to equation 2.10 is given by the Green Function

$$\mathcal{G}_\omega(t, t') \;=\; \pi N_\omega(t) N_\omega(t') \left[Ai(z(t))\overline{Bi}(z(t')\theta(t - t') + t \leftrightarrow t'\right], \tag{2.11}$$

with

$$\overline{Bi}(z(t)) \;=\; Bi(z(t)) + \cot\left(\phi(\omega)\right) Ai(z(t)). \tag{2.12}$$

Here $Ai(z)$ and $Bi(z)$ denote the two independent Airy functions. The function $\phi(\omega)$ is defined as

$$\phi(\omega) \;=\; s_\omega(t_0) + \frac{\pi}{4} - \eta_{np}(\omega, t_0) \tag{2.13}$$

with $\eta_{np}(\omega)$ being a non-perturbative phase, fixed at some small $t_0$. From 2.11 and 2.12 it follows, as discussed in ref. [1], that the BFKL Green function has poles when

$$\phi(\omega) = n\pi, \quad n = \; 0,\; 1,\; 2,\; 3 \;\ldots\; . \tag{2.14}$$

The equations 2.14 and 2.13 define the eigenvalues $\omega_n$, which are a function of the non-perturbative boundary condition $\eta_{np}(n)$.

Furthermore in [1] we have shown that, in case of positive $\omega_n$, the eigenfunctions of the BFKL operator are given by

$$f_{\omega_n}(t) \;=\; \sqrt{\frac{\pi}{\phi'(\omega_n)}} N_{\omega_n}(t) Ai(z(t)), \tag{2.15}$$

whith $N_{\omega_n}(t)$ being the normalisation factor, which is given by

$$N_\omega(t) \;=\; \frac{|z(t)|^{1/4}}{\sqrt{\frac{1}{2}\bar{\alpha_s}(t)\chi'\left(\nu_\omega(t)\right)}}\;. \tag{2.16}$$

Here $\chi$ denotes the BFKL characteristic function which in LO is simply equal to $\chi_0$ but is more complicated in NLO.

When the Airy function in equation 2.15 is asymptotically expanded at $t = t_0$, far away from $t_c$, we obtain

$$f_{\omega_n}(t_0) \;\propto\; Ai(z(t_0)) \;\approx\; \frac{1}{\sqrt{\pi}\;|z(t)|^{1/4}} \sin\left(s_\omega(t_0) + \frac{\pi}{4}\right). \tag{2.17}$$

This means that the function $\phi$ is the difference between the perturbative and non-perturbative phases of the wave function, which should not depend on $t_0$. [2]

In case of negative values of $\omega$ the equation 2.7 is never fulfilled, i.e. there is no critical point and no quantization of eigenvalues. The negative $\omega$ eigenfunction were derived in ref. [1] and are given by

$$f_{-|\omega|}(t) \;=\; \sqrt{\frac{2}{\pi}} \frac{1}{\sqrt{\bar{\alpha_s}(t)\chi'\left(\nu_\omega(t)\right)}} \sin\left(\int_{t_0}^{t} \nu_\omega(t')dt' + \eta_{NP}\right). \tag{2.18}$$

The eigenfunction defined by eq. 2.15 and 2.18 fulfil the completeness relation

$$\lim_{\omega_{min}\to-\infty} \int_{\omega_{min}}^{0} d\omega f_{-|\omega|}(t) f^*_{-|\omega|}(t') + \sum_{n=1}^{\infty} f_{\omega_n}(t) f_{\omega_n}(t') \;=\; \delta(t-t') \tag{2.19}$$

and are orthonormal, as shown in [2].

[2] Although we call this phase no-perturbative we are fixing it in the perturbative region, at $t_0$ equivalent to $k_0 = 1$ GeV, close to $\Lambda_{QCD}$. At this $k_0$ the value of $\bar{\alpha_s}$ is 0.50.

# 3 NLO evaluation

To obtain the eigenfunction of the BFKL equation in NLO we need just to replace eq. 2.5 by its NLO counterpart

$$\omega \;=\; \bar{\alpha_s}\chi_0(\nu) + \bar{\alpha_s}^2\chi_1(\nu) + \mathcal{O}(\bar{\alpha_s}^3) \tag{3.1}$$

where $\chi_0(\nu)$ and $\chi_1(\nu)$ are the LO and NLO characteristic functions respectively. The NLO value of $\alpha_s$ was fixed by measurement at $Z^0$ pole. In our numerical analysis, we modify $\chi_1$ following the method of Salam [7] in which the collinear contributions are resummed, leaving a remnant which is accessible to a perturbative analysis. For the analysis of this paper we use Scheme 3 of the Salam paper, see Appendix A.

To create the eigenfunction we have chosen the value of $t_0$ equivalent to $k_0 = 1$ GeV, close to $\Lambda_{QCD}$ but still in the perturbative region, with $\bar{\alpha_s}(k_0) = 0.50$. To be able to describe the measured structure function $F_2$, which has a changing slope $\lambda$, $\eta_{np}$ should vary with $n$ and the value of the non-perturbative phase $\eta_{np}$ for the leading eigenfunctions should be close to zero, see the discussion in Section 4.1 and 4.3. We adopted therefore the convention that $n$ in equation 2.14 should be counted from 1 and $\eta_{np}$ should stay in the interval between $+\pi/4$ and $-3\pi/4$.[3] The values of $\eta_n$ and the corresponding eigenfunctions, used later in the fit, are not limited to this interval. They are obtained from the periodicity of $\eta_n$, i.e. by adding (or subtracting) multiples of $\pi$ on both sides of equation 2.13. In the following we will label the eigenvalues and eigenfunctions with $n \geq 1$ and call the $n$ dependent phase $\eta_{np}(n)$ just $\eta_n$.

In Fig. 2 we display the eigenvalues $\omega_n$ obtained from eq. 3.1, using three different non-perturbative phases, $\eta_n = 0, \pi/4, -\pi/4$. The dotted line shows, taking as example the $\eta_n = 0$ case, that the dependence of $\omega_n$ values from $n$ (for $n > 1$) can be simply parametrised by

$$\omega \;=\; \frac{A}{n+B}\;, \tag{3.2}$$

as noticed already in [3]. For $\eta_n = 0$ we found in NLO, that A = 0.52223, B= 1.62001. Since we apply this parametrisation below to describe data we recall its derivation following ref. [3]. In LO we can integrate $s_\omega(t_0)$ by parts

$$s_\omega(t_0) \;=\; \int_{t_0}^{t_c} \nu_\omega(t')dt' = -\nu_\omega(t_0)t_0 + \frac{1}{\bar{\beta_0}\omega}\int_0^{\nu_\omega(t_0)} \chi_0(\nu')d\nu', \tag{3.3}$$

where in the last step we used the LO relation $t = \chi_0(\nu)/\bar{\beta_0}\omega$. For $\omega$ values approaching 0, we have

$$\chi_0\left(\nu_\omega(t)\right) \;=\; \frac{\omega}{\bar{\alpha_s}(t)} \to 0 \tag{3.4}$$

Therefore, for small $\omega$ and small $t_0$, $\nu_\omega$ is quickly approaching its asymptotic value, $\nu_0$, with $\chi_0(\nu_0) = 0$. In this limit $\int_0^{\nu_\omega(t_0)} \chi_0(\nu')d\nu'$ and $\nu_\omega(t_0)$ becomes independent of $\omega$ and eq. 2.13

[3]Note that with $n = 1$ and $\eta_{np} = 0$ the equation 2.13 is well satisfied, however it is not satisfied with $n = 0$ and $\eta_{np} = 0$, since $s_\omega(t_0)$ is always positive. The periodicity of equation 2.13 assures that the same eigenfunction is obtained with $n = 1$ and $\eta_{np} = 0$ as with $n = 0$ and $\eta_{np} = \pi$.

implies that

$$n\pi \ = a + \frac{b}{\bar{\beta}_0 \omega} + \frac{\pi}{4} - \eta_n, \tag{3.5}$$

where $a, b$ are constants independent of $\omega$, what leads to the relation 3.2. In NLO this relation is satisfied already for $n \geq 2$, since $\nu_\omega(t_0)$ is less dependent from $\omega$ then in LO. The relation 3.2 indicates also that $t_c = \chi_0(0)/\bar{\beta}_0\omega_n$ should grow almost linearly with $n$, for larger $n$. This is also a feature of the NLO computation, see Fig.3. The value of $t_c$ is related to the value of the critical momenta $k_c$ by $t_c = \ln k_c^2/\Lambda_{QCD}^2$ with $\Lambda_{QCD} = 275$ MeV.

In Fig. 4 we show as example the first three different eigenfunctions 1,2 and 3, computed from eq. 2.15 and 3.1, at phases $\eta_n = 0, \pi/4, -\pi/4$.

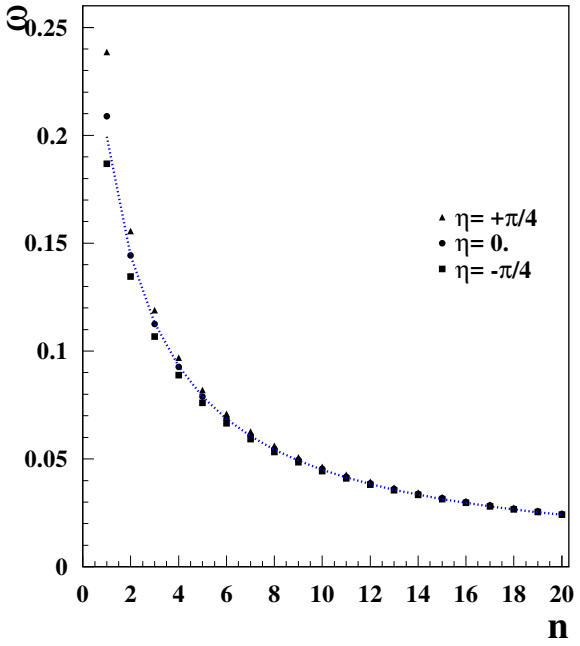


Figure 2: Eigenvalues $\omega_n$ determined in NLO for three fixed non-perturbative phases, $\eta_n$. The dotted line shows a simple parametrisation described in the text.

# 4 Application to data

To apply the BFKL Green Function to data we express the low-$x$ structure function of the proton, $F_2(x, Q^2)$, in terms of the discrete BFKL eigenfunctions by

$$F_2(x, Q^2) \ = \ \int_x^1 d\zeta \int \frac{dk}{k} \Phi_\gamma(\zeta, Q, k) x g\left(\frac{x}{\zeta}, k\right), \tag{4.1}$$

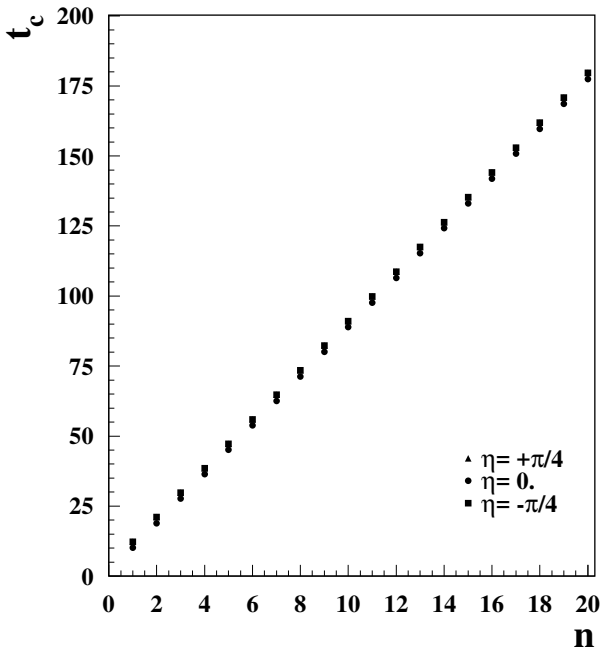


Figure 3: The critical momenta $t_c$ determined in NLO for three fixed non-perturbative phases, $\eta_n$. $t_c = \ln k_c^2/\Lambda_{QCD}^2$ with $\Lambda_{QCD} = 275$ MeV.

where $xg\left(\frac{x}{\zeta}, k\right)$ denotes the unintegrated gluon density

$$xg(x,k) \;=\; \int \frac{dk'}{k'}\Phi_p(k')\left(\frac{k'\,x}{k}\right)^{-\omega_n} k^2\left(\sum_n f^*_{\omega_n}(k')f_{\omega_n}(k) + \int_{-\infty}^{0} d\omega x^{-\omega} f_{-|\omega|}(t) f_{-|\omega|}(t')\right) \tag{4.2}$$

and $\Phi_p(k)$ denotes the impact factor that describes how proton couples to the BFKL amplitudes at zero momentum transfer. The impact factor, $\Phi_\gamma(\zeta, Q, k)$, which describes the coupling of the virtual photon to the eigenfunctions is given in [6]; the dependence on $\zeta$ reflects the fact that beyond the leading logarithm approximation, the longitudinal momentum fraction, $x$, of the gluon differs from the Bjorken-value, determined by $Q^2$. $\Phi_\gamma(\zeta, Q, k)$ of Ref. [6] is determined taking into account kinematical constraints allowing for non-zero quark masses. The $(k'/k)^{\omega_n}$ factor arises from a mismatch between the "rapidity", $Y$, of the forward gluon-gluon scattering amplitude used in the BFKL approach

$$Y \;=\; \ln\left(\frac{s}{kk'}\right)$$

and the logarithm of Bjorken $x$, which is given by

$$\ln\left(\frac{1}{x}\right) \;=\; \ln\left(\frac{s}{k^2}\right).$$

This ambiguity has no effect in LO but in NLO it can be compensated by replacing the LO characteristic function $\chi_0(\nu)$ by $\chi_0(\omega/2, \nu)$, which modifies the NLO characteristic function

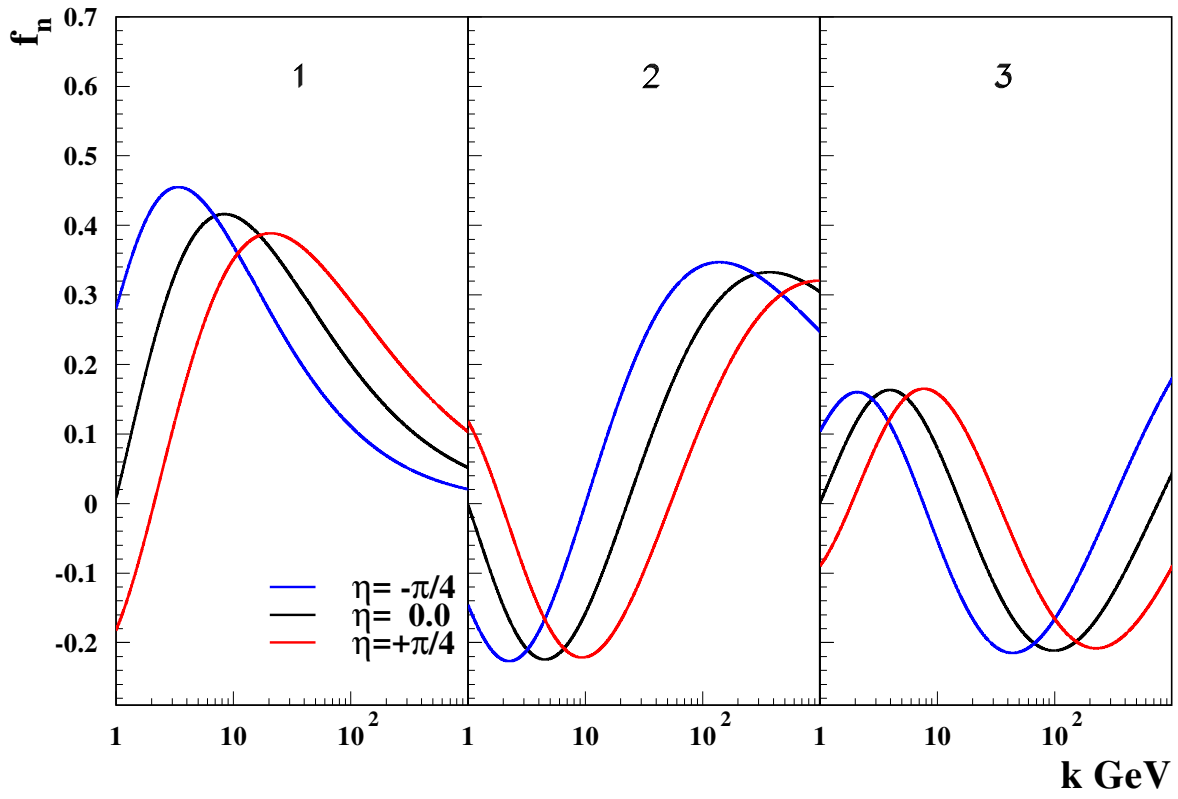


Figure 4: The first three eigenfunctions computed for three fixed non-perturbative phases, $\eta_n$.

$\chi_1$, see Appendix A.

The proton impact factor is determined by the confining forces. It is therefore barely known, besides the fact that it should be concentrated at the values of $k < \mathcal{O}(1)$ GeV. We use here a simple parametrisation in the form

$$\Phi_p(\mathbf{k}) \;=\; A\, k^2 e^{-bk^2}, \tag{4.3}$$

which vanishes at small $k^2$ as a consequence of colour transparency, is everywhere positive and decreases for large transverse momentum. Since the range of the proton form factor is much smaller than the oscillation period of the BFKL eigenfunctions we do not expect that the results should have substantial sensitivity to a value of $b$.

## 4.1 Properties of HERA data

The HERA $F_2$ data in the low $x$ region can be simply parametrised by $F_2 = c\ (1/x)^\lambda$, with the constants $c$ and $\lambda$ being a function of $Q^2$, see e.g. [9]. When $Q^2$ changes from 4 GeV$^2$ to 100 GeV$^2$ $\lambda$ changes from about 0.15 to 0.3. The BFKL evaluation of $F_2$, which assumes that $\eta_n$ is independent of $n$, would predict that $\lambda$ is a constant *independent* of $Q^2$ with $\lambda \approx \omega_1$, since it is the first pole which dominates $F_2$, when the value of $\eta_n$ is fixed. Therefore, the only way to make $\lambda$ dependent of $Q^2$ is to make $\eta_n$ *dependent* of $n$. Otherwise, the predicted value of $\lambda$ will be about 0.25, *independent* of $Q^2$, see Fig.2, in clear contradiction to HERA data.

We used for fits the highest precision HERA data [8] given in terms of reduced cross sections from which we extracted the $F_2$ values, using the assumption that $F_L$ is proportional to $F_2$. We also limited the $y$ range to avoid possible complications of larger $F_L$ contribution, see e.g. [9]. Since we are focusing on the comparison with the $F_2$ measurements we use here only the 920 GeV data set of [8]. We also limited the comparison with data to the region $x < 0.001$ and $Q^2 > 6$ GeV$^2$ since the BFKL equation is valid at very low $x$ only. The $Q^2$ cut was chosen to be relatively high to avoid any complications due to possible saturation corrections [10]. The number of experimental points used for fits was then $N_p = 51$. (It represents around 1/3 of the whole low $x$ data sample, defined as $x < 0.01$, $Q^2 > 3$ GeV$^2$).

We used for this investigation the uncorrelated errors only, obtained by adding in quadrature all the correlated errors of ref. [8]. From the data analysis of ref. [10] we know that the uncorrelated errors overestimate the error sizeably, so that the $\chi^2/N_{df}$ of a good fit should be around 0.7, instead of about 1 as in case of correlated errors, see also [12].

## 4.2 Boundary condition

The challenge of data description with BFKL is to find a simple boundary condition, i.e., $\eta - n$ relation, which would lead to a precise description of data. At the beginning we tried to parametrise $\eta$ as a function of $n$, using polynomial or other functional dependences. This failed because we were not able to find any functional dependence which would lead

to $\chi^2 < O(500)$. In the next step we tried to find a set of $\eta_n$ (with $n =, 1, 2, 3...10$) values using only some assumptions of local continuity. This was essentially a 10 parameter fit, with some limitations. After a longer search, using permutational methods to avoid any pre-conceptional bias on the form of $\eta - n$ relation, we found a set of 10 $\eta_n$ values which gave an acceptable $\chi^2 \approx 40$. Studying this set we noticed that it can be well parametrised by an $\omega - n$ relation, similar to eq.3.2,

$$\omega \;=\; \frac{A}{n+B} + C \;, \tag{4.4}$$

with a $C$ value which is very small, but different from 0. The $\eta_n$ values were then obtained from eq. 2.13 and 2.14, by

$$\eta_n \;=\; s_{\omega_n}(t_0) + \frac{\pi}{4} - n\pi. \tag{4.5}$$

The parameters $A$, $B$ and $C$, together with $\eta_{neg}$, the phase of the negative omega contribution, were considered as free parameters of the fit, which we call in the following the ABC-Fit. In addition to these four parameters the overall normalisation was also fitted to data.

As we observed that the system was exhibiting a multitude of local optima, we used the Bayesian Analysis Toolkit (BAT) [11] to find the global optimum. BAT generates samples in the parameter space via Markov chain Monte Carlo (MCMC), distributed according to the posterior probability of the parameters. The best fit value is the parameter set with the highest posterior probability, respectively the lowest $\chi^2$-value. Fig. 5 shows a marginalised distribution of the $ABC$-Fit, for the variables, $B$ and $C$. The regions of higher probability are shown as coloured areas, with probability increasing as colour changes from blue over green to yellow. The small circle shows the position of the best fit, given in Table 1. The complicated structure of the probability distribution is also seen as a function of $A$ and $B$ variables, see Fig. 6

Figures 5 and 6 show that the distribution of probability has a complicated structure; there are several extended regions of higher probability, which are completely disconnected. In this situation the usual fitting methods, based on MINUIT, are poorly working, since they are assuming a steady increase of probability towards the real minimum.

Using the BAT and using the above parametrisation we found an excellent agreement with data, $\chi^2/N_{df} \approx 33/46$. We performed this fit for several specific values of the parameter $b$ of $\Phi_p$ and found that the $\chi^2$ values were the same, within the computational precision of the fit, $\Delta\chi^2 = \pm 1$. For each value of $b$ the values of the fit parameters, $A, B, C$ and $\eta_{neg}$, were somewhat different and compensated the change of $b$, see as example Table 1. The values of the $A$ and $B$ parameters are in the usual range, $A \approx 0.5$, $B \approx 1.5$, similar to the values at a fixed $\eta$ phase, see eq. 3.2 and below. The third parameter, $C$, is very small, O($10^{-3}$), i.e. much smaller than the value of the smallest eigenvalue, $\omega_{20} \approx 0.025$, used in the fit.

In spite of the fact that $C$ is very small, it is impossible to put its value to zero without seriously deteriorating the quality of the $ABC$ fit (to $\chi^2 \approx 150$). In the standard QCD we should expect that $C$ should be zero and $\omega_n \to 0$ when $n \to \infty$, as in the LO calculation discussed above. After a while we noticed though, that the parameter $C$ can to be put to

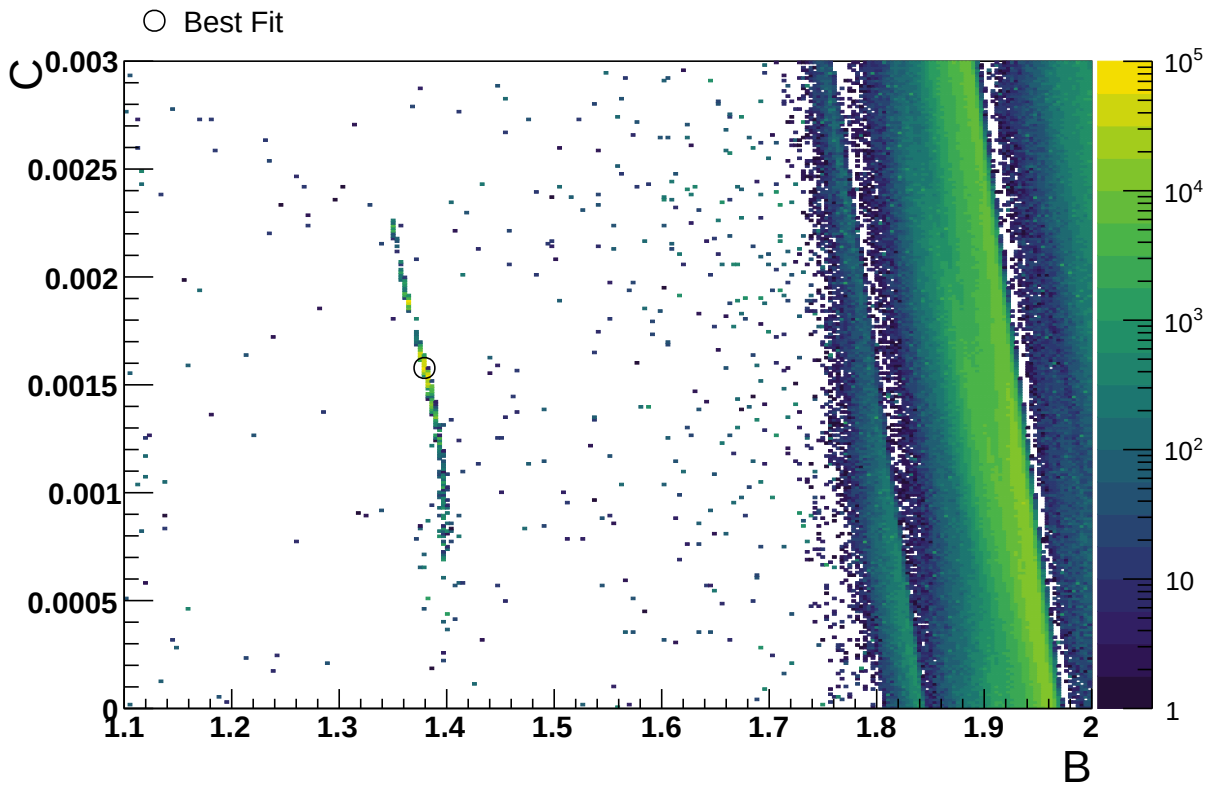


Figure 5: Probability density of the $ABC$ fit as a function of the B and C parameters. The legend shows the probability scale in arbitrary units

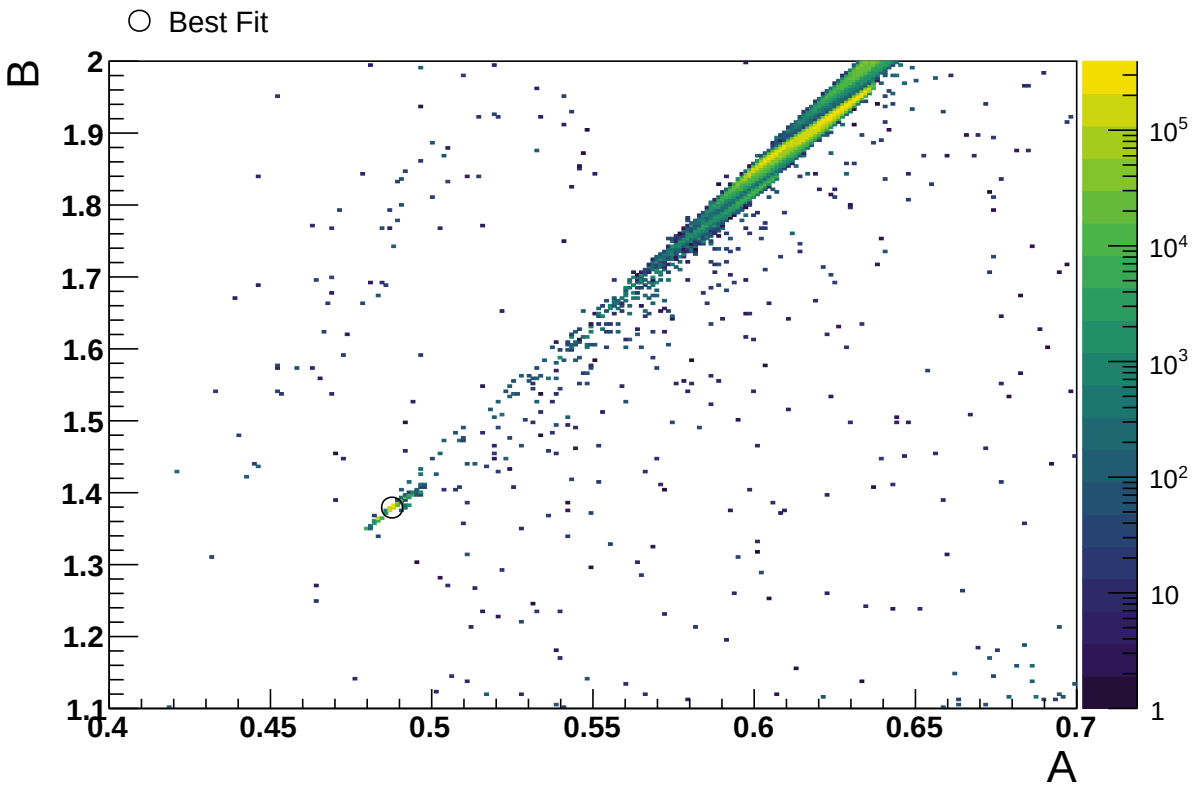


Figure 6: Probability density of the *ABC*-Fit as a function of the B and A parameters. The legend shows the probability scale in arbitrary units

| $b$ (GeV$^{-2}$) | 10 | 20 |
|---|---|---|
| $A$ | 0.48771 | 0.47905 |
| $B$ | 1.37933 | 1.34020 |
| $C$ | 0.001578 | 0.002424 |
| $\eta_{neg}$ | -0.0754 | -0.0518 |
| $\chi^2$ | 32.9 | 33.1 |

Table 1: Results of the ABC-Fit to 51 data points with $x < 0.001$ and $Q^2 > 6$ GeV$^2$.

zero if we let $\eta_1$, the phase of the first eigenfunction, to be a free parameter, instead of $C$. The fits obtained in this way are of the same quality as the $ABC$ fits, they have however an unexpected property; the value of the $\eta_1$ parameter is always chosen such that the first eigenfunction decouples (or nearly decouples) from the proton. This means that its overlaps with the proton form-factor becomes zero (or nearly zero), independent of the choice of $b$. We call this fit the AB-Fit and give its results in Table 2 for two values of $b$ as example. Note that the value of $\eta_1$ is effectively not a free parameter in this fit.

| $b$ (GeV$^{-2}$) | 10 | 20 |
|---|---|---|
| $A$ | 0.51844 | 0.51913 |
| $B$ | 1.58697 | 1.58657 |
| $\eta_{neg}$ | -0.0911 | -0.0550 |
| $\chi^2$ | 33.9 | 33.3 |

Table 2: Results of the AB-Fit to 51 data points with $x < 0.001$ and $Q^2 > 6$ GeV$^2$.

The results shown here for the AB and ABC fits used 20 eigenfunctions, to see the convergence, see below. In the AB-Fit the first eigenfunction is not used since it is decoupling from the proton. The decoupling happens at $\eta_1 = 0.0707$ for the $b = 10$ and $\eta_1 = 0.0503$ for the $b = 20$ GeV$^2$ case. In addition we note that an approximate decoupling happens also in the ABC-Fit, where the contribution of the first pole is much smaller than that of the second one, by more than a factor of 10.

The assumption of decoupling of the first eigenfunction together with the AB-relation of eq. 3.2 leads to a much simpler probability structure, see Figure 7, with a steady increase of probability towards one minimum, i.e., without a multitude of local minima.

In Fig. 8 we show the $\eta - n$ relation as computed from the parameters $A, B$ of the AB-Fit for two values of $b$. Note that $\eta - n$ relation is visibly different in the two cases, although the parameters $A, B$ differ by a fraction of per mill only. In Fig. 9 we show the same relation as computed from the parameters $A, B, C$ of the ABC-Fit for the same two values of $b$. Note that the $\eta - n$ relation is simpler in the AB-Fit than in the ABC-Fit.

In general, we observe that the AB and ABC parameterisations are characterised by a high sensitivity to the $\omega$ values. The values of the parameters $A, B$ for the case of constant $\eta$, given below eq. 3.2, differ only by about a percent from the values of Table 2, and yet

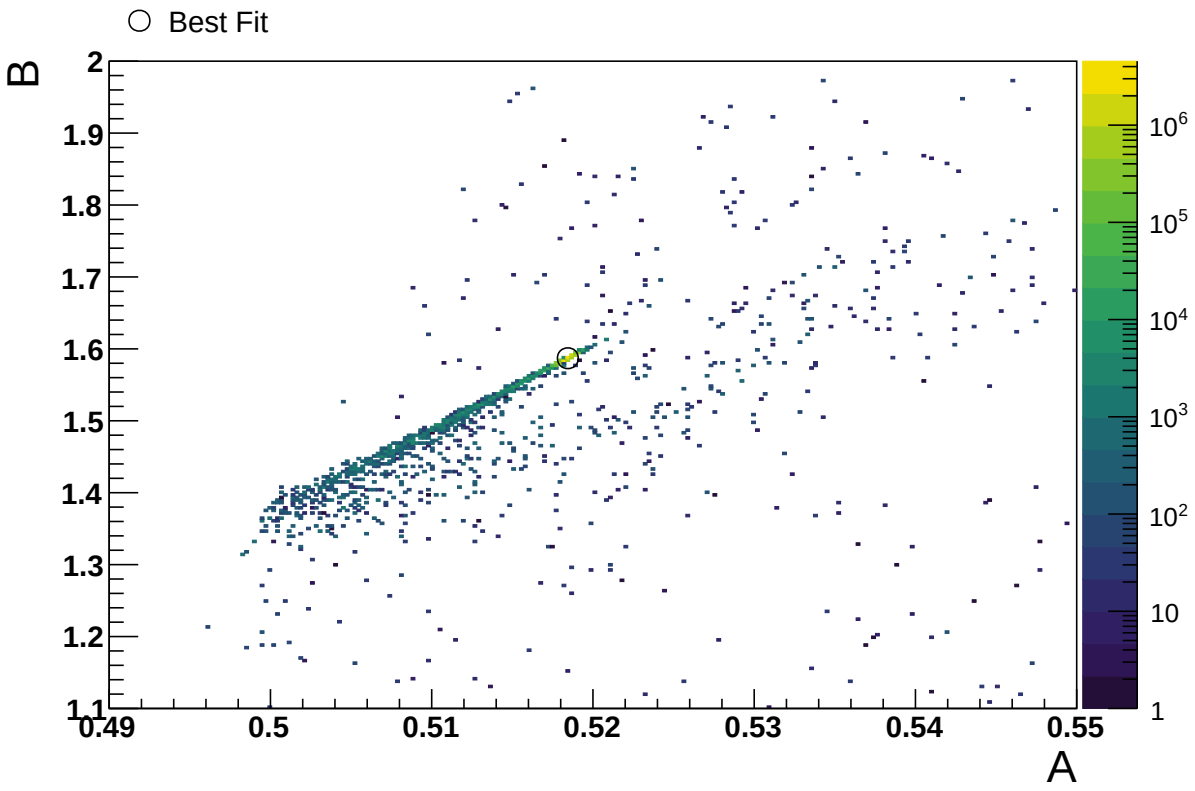


Figure 7: Probability density of the $AB$-Fit as a function of the B and A parameters. The legend shows the probability scale in an arbitrary units

produce a very different $\eta - n$ relation; a fit to data with $\eta = const$ would give $\chi^2 \approx 3000$!

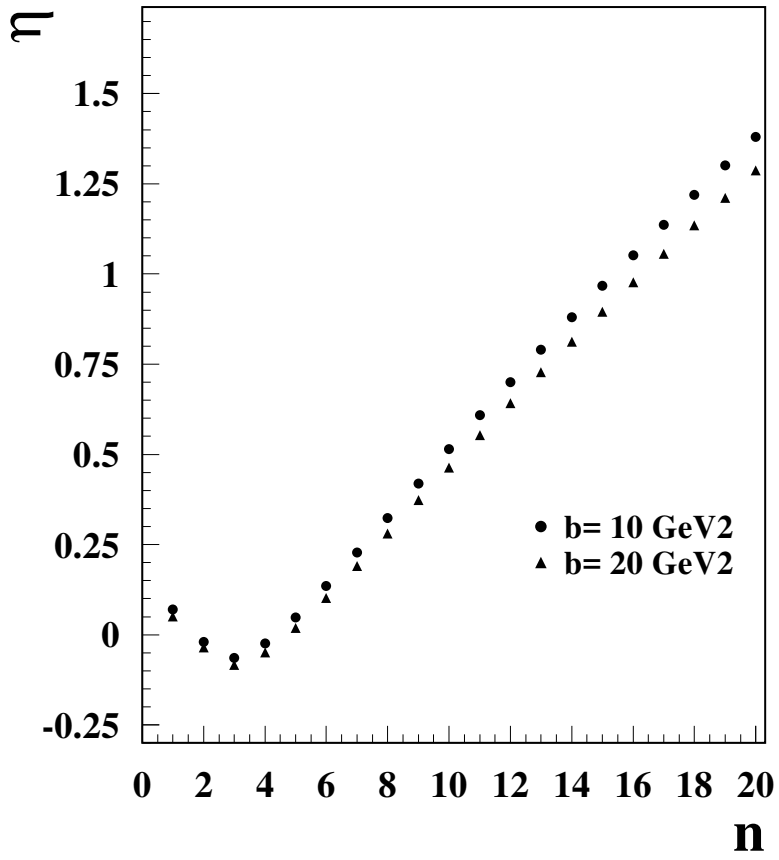


Figure 8: $\eta - n$ relation as computed from the parameters $A, B$ of the AB-Fit.

## 4.3 Fit results

In Fig. 10 we show the comparison of the AB-Fit results with data (with $b = 10$ GeV$^2$). Figure shows a very good agreement, corresponding to the excellent $\chi^2$ value. The results obtained with different choices of parameter $b$, or with ABC-Fit, would look the same in this figure.

The discrete BFKL is able to describe the $Q^2$ dependence of the slope $\lambda$, although neither the eigenfunctions nor the AB(C)-relation are $Q^2$ dependent. In Fig. 11 we show the comparison of the $\lambda$ parameter obtained from the AB-Fit with data. The $\lambda$ parameter was determined in the very low $x < 0.001$ region and in the $Q^2$ range between 6.5 and 35 GeV$^2$. The $Q^2$ dependence of the $\lambda$ parameter enters indirectly through the choice of the $\omega - n$ relation.

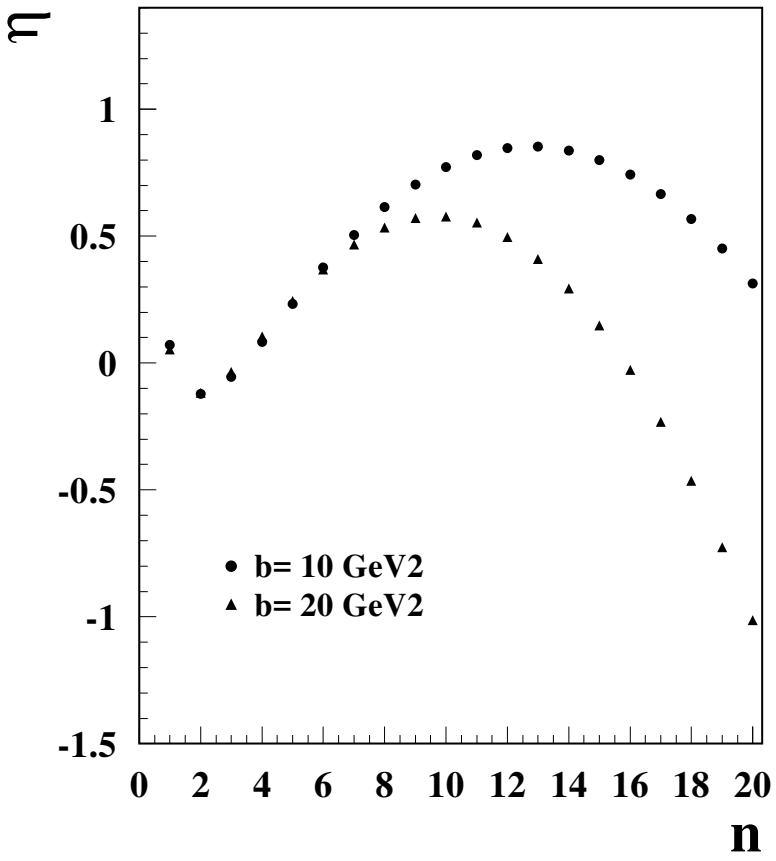


Figure 9: $\eta - n$ relation as computed from the parameters $A, B, C$ of the ABC-Fit.

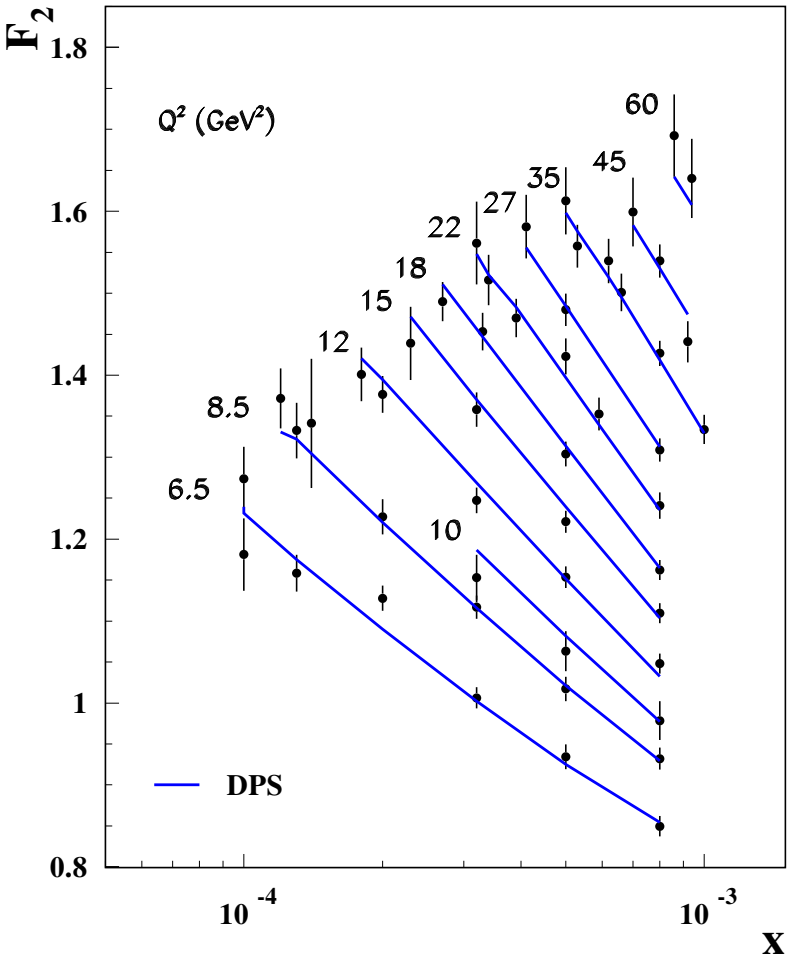


Figure 10: Comparison of the $AB$ fit results with data

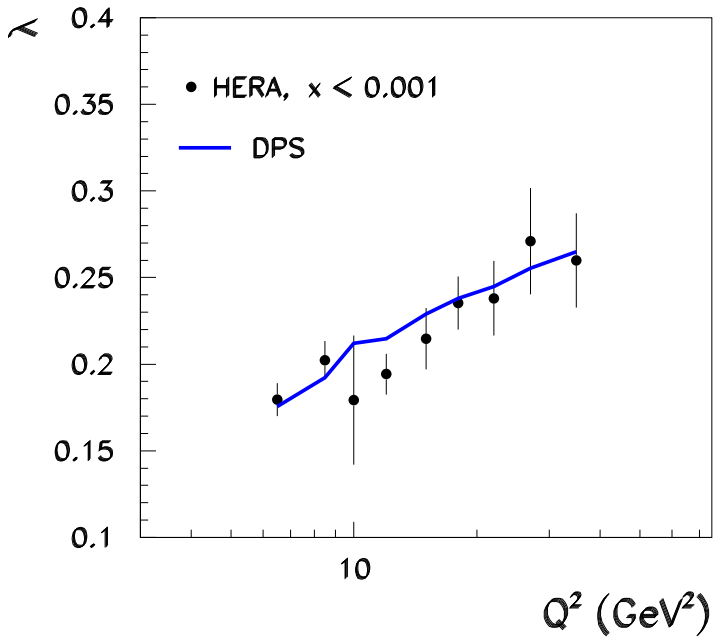


Figure 11: Comparison of the $\lambda$ parameter, obtained in the $AB$ fit, with data.

## 4.4 Discussion of the phase tuning mechanism

The choice of the $\omega - n$ relation determines the set of phases $\eta_n$ which tune the contributions of the individual eigenfunctions to describe the data. To see how it happens we display in Fig. 12 the eigenfunctions 1, 2, 3, and as example of subleading ones the eigenfunctions 7, 8, 9, as a function of $k$. The eigenfunctions are plotted with the $\eta_n$ phases, for $n \geq 2$, given by the AB-Fit. The first eigenfunction has the phase $\eta_1$, which zeroes its overlap with the proton form factor. Figure shows that the leading eigenfunctions 2 and 3 have the values $f_n(k_0) \approx 0$, whereas the eigenfunctions 7, 8 and 9, have the values at $k_0$ which are substantially different from zero.

To see more precisely how the phases determine the overlaps we display in Fig. 13 the eigenfunctions 1, 2 and 3 in the region close to $k_0$. We see that the eigenfunction 1 starts negative at $k_0 = 1$ GeV but then crosses zero at $k_0 \approx 1.05$ and becomes positive. This small negative region is sufficient to nearly zero the overlap with the proton form factor and effectively cancel its contribution to $F_2$. The eigenfunction 2 and 3 are not crossing zero, and in both cases the proton and photon overlap have the same signs. They give, therefore, large contributions to $F_2$. The contributions of the subleading eigenfunctions 7, 8 and 9 are also significant because $\eta_n$ values are substantially different than zero, $\eta_7 = 0.23$, $\eta_8 = 0.32$ and $\eta_9 = 0.42$. This leads to large overlaps with the proton and photon form factor, which have opposite signs. Their contributions to $F_2$ are therefore relatively large, have negative sign and so can change the slope $\lambda$.

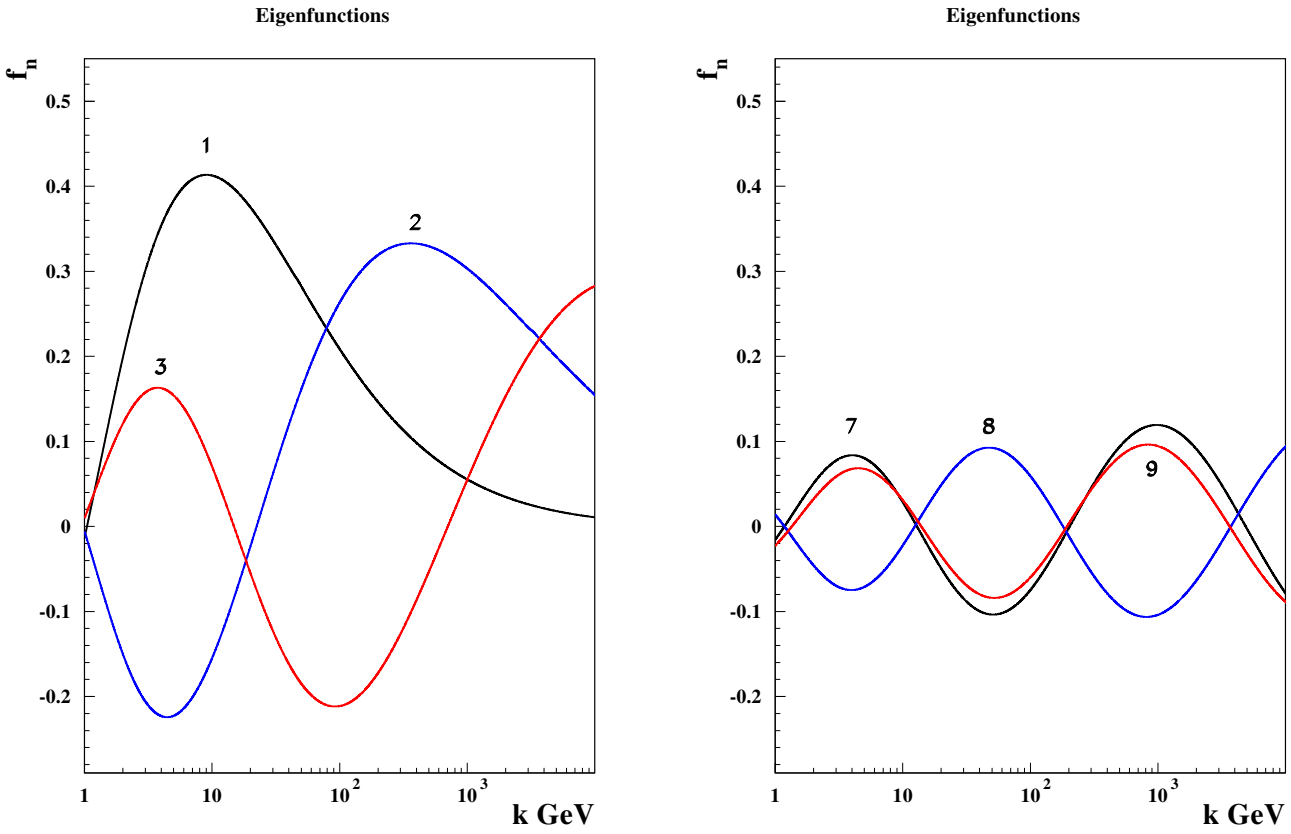


Figure 12: Eigenfunctions 1, 2, 3, and 7, 8 and 9 in the $k$ region accessible to experiments. The eigenfunctions are plotted with the $\eta_n$ phases given by the $AB$ fit. The first eigenfunction is plotted with the phase which which decouples it from the proton.

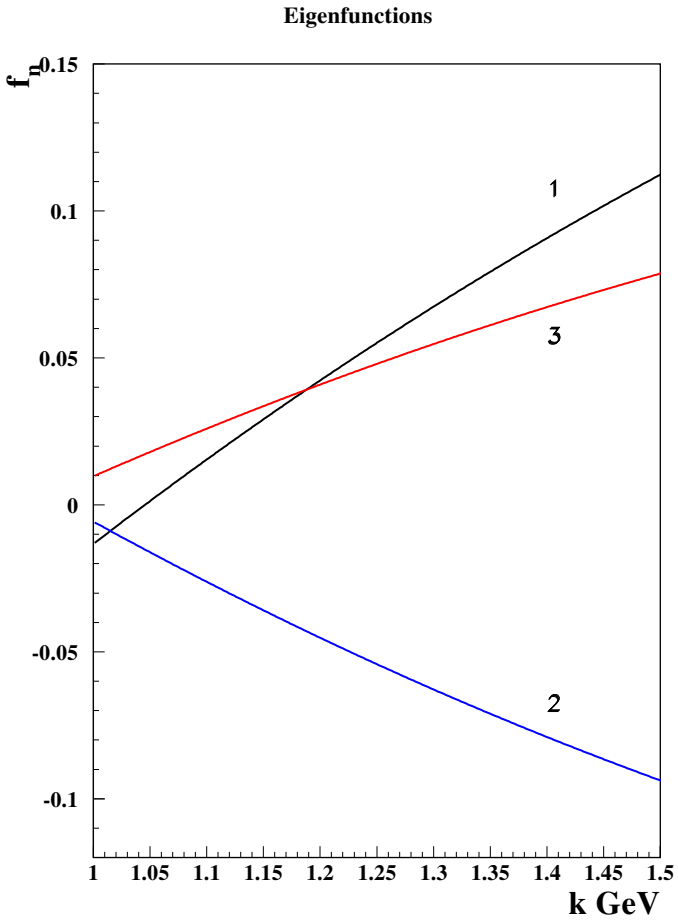


Figure 13: Eigenfunctions 1, 2, 3, in the $k$ region close to $k_0$. The eigenfunctions are plotted with the $\eta_n$ phases given by the $AB$ fit. The first eigenfunction is plotted with the phase which gives zero overlap with the proton form factor.

Figure 14 shows the contributions to $F_2$ of individual eigenfunctions, on the example of results at $Q^2 = 6.5$ and 35 GeV$^2$. The larger dots show the measured points, the full blue lines show the BFKL prediction for $F_2$, the same as in Fig. 10. Other lines show the contributions of eigenfunctions specified in the legend, i.e. the terms

$$F_2^{(n)}(x,Q^2) \;=\; \int_x^1 d\zeta \int \frac{dk}{k}\Phi_{\rm DIS}(\zeta,Q,k)\int \frac{dk'}{k'}\Phi_p(k')\left(\frac{k'\,x}{k}\right)^{-\omega_n} k^2 f^*_{\omega_n}(k')f_{\omega_n}(k) \qquad (4.6)$$

With exception of the contributions of the second and of the continuous negative $\omega$ terms, the contributions of other eigenfunctions are displayed as a sum of two eigenfunctions, (3+4), (5+6), ... (19+20), to simplify the picture. The black full line shows the contribution of the second, leading eigenfunction, which is substantially larger than $F_2$.

The contribution of the second eigenfunction, together with the contribution (3+4) and the negative $\omega$ one, is positive. The contributions of the eigenfunctions 5 to 20 are all negative. The negative contributions correct the positive one to reproduce precisely the measured $F_2$. In this way the effective slope is also changed; the contribution of the dominating, second term, which has $\omega_2 = 0.144$, is modified to $\lambda = 0.176$ at $Q^2 = 6.5$ GeV$^2$ and $\lambda = 0.265$ at $Q^2 = 35$ GeV$^2$, in agreement with data. Note that the corrections at $Q^2 = 35$ GeV$^2$ are much larger than at $Q^2 = 6.5$ GeV$^2$ due to the increased overlap with the DIS form factor. Note also that the sub-leading terms have to converge more slowly than the eigenfunctions itself to obtain the variation of $\lambda$ in BFKL. Nevertheless, we see from Fig. 14 that the contributions of eigenfunctions with $n > 16$ start to approach zero., i.e. show convergence.

Summarising we can tell that the excellent description of data is achieved by a fine tune of the non-perturbative phases $\eta_n$. This phase tune is a results of a simple $\omega - n$ relation which is well motivated in BFKL and is driven by only two or three parameters.

## 4.5 Decoupling of the first eigenfunction

The decoupling of the first eigenfunction is an unexpected and puzzling feature of this investigation. Therefore, we have also checked that the results are not depending on the number of eigenfunction which we use in the fit. In Table 3 we show the results of fits made with the first 20, 16, 12 and 10 eigenfunctions. All the fits were made with the ABC relation and the phase of the first eigenfunction fixed at the decoupling point.

All the fits which we performed show clearly that the first eigenfunction decouples or nearly decouples, irrespectively of the number of eigenfunctions used in the fit or the assumed value of the proton form factor. From the technical point of view this (near) decoupling happens because the position of the critical point of the first eigenfunction is close to the physical region, $k_c(1) \approx 50$ GeV, whereas the critical point of the subsequent eigenfunctions is far away from it, $k_c(2) \approx 3,3$ TeV, $k_c(3) \approx 270$ TeV, $k_c(4) \approx 20000$ TeV, etc. Therefore, the first eigenfunction varies more quickly near $k_0$ than the subsequent ones, so that very small change of the $\eta_1$ phase lead to a large change of the first contribution.

As seen in Fig. 13, the decoupling of the first eigenfunction can only happen because there is a transition from the negative to positive values in a region close to the starting

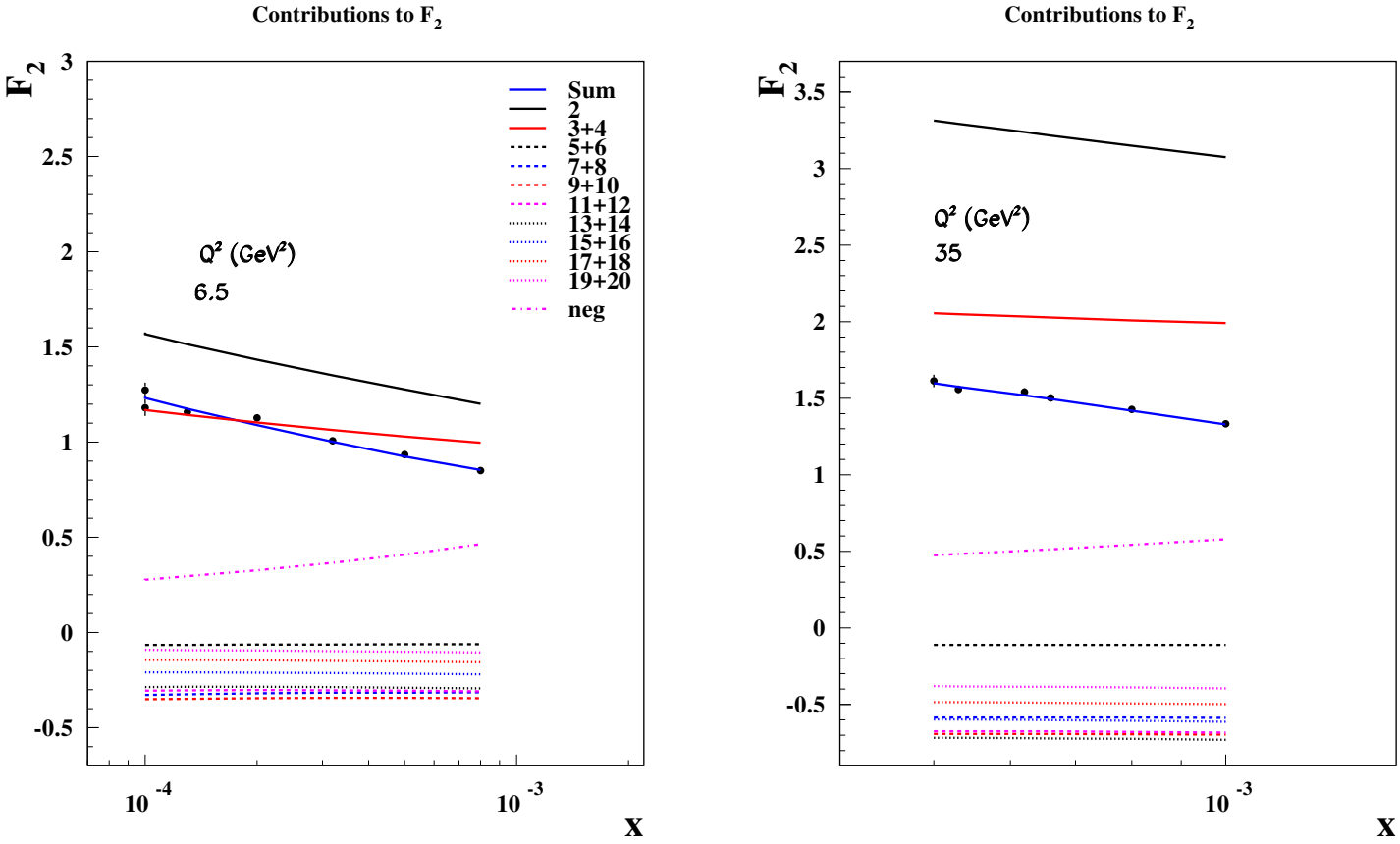


Figure 14: Contributions to $F_2$ of individual eigenfunctions. The dots show the measured points at $Q^2 = 6.5$ and 35 GeV$^2$, The full blue line shows the BFKL prediction at these $Q^2$'s, other lines show the contributions of eigenfunctions specified in the legend. With exception of the second eigenfunction and the continuous negative $\omega$ contributions, the contributions of the eigenfunctions are displayed as a sum of two eigenfunctions, (3+4), (5+6), ... (19+20).

| $N_{ef}$ | 20 | 16 | 12 | 10 |
|---|---|---|---|---|
| $A$ | 0.51768 | 0.47904 | 0.44987 | 0.42753 |
| $B$ | 1.58209 | 1.32672 | 1.16597 | 1.95858 |
| $C$ | 0.000037 | 0.002092 | 0.00431 | 0.00586 |
| $\eta_{neg}$ | -0.0895 | -0.0723 | -0.0738 | -0.0770 |
| $\chi^2$ | 33.4 | 34.0 | 34.4 | 34.7 |

Table 3: Results of the ABC-Fit performed with different number of eigenfunctions, $N_{ef}$. All fits were using the same 51 data points, with $x < 0.001$ and $Q^2 > 6$ GeV$^2$. The value of the proton form factor was $b = 10$ GeV$^2$.

point $k_0$. Such a transition is a clear indication that the first eigenfunction, chosen by the fit, cannot be a wave function of a ground state. As shown in Appendix B, the wave function of the BFKL ground state has to be completely positive. Therefore, the decoupling of the first eigenfunction could be interpreted as an indication that there exist an additional ground state, corresponding to $n = 0$.

Our computation gives us though some hints about the properties of such a state. From the values of the turning points, $t_c(n)$, which are almost linearly growing with $n$, Fig. 3, we can estimate the $k_c$ value of the ground state, $n = 0$, as being around 500 to 700 MeV, [4] well below our starting value of $k_0 = 1$ GeV. Such a state would have a high intercept, $\omega_0 \approx 0.3$, and would not have any oscillations above $k_0$, it would just be exponentially decaying with increasing $\ln(k)$. It was already pointed out by Gribov [15] that such a bare pomeron state should be renormalised in the framework of the reggeon calculus and that its effective intercept may become small, as in the soft pomeron case.

Indeed, the $k_c$ value of the additional ground state, of 500 to 700 MeV, lays right in the middle of the saturation region [16–23], where multiple pomeron exchanges should dominate [24]. In our approach, these exchanges would almost entirely involve the interaction of the low $k_c$ ground state with itself, since its size is much larger than the size of higher eigenfunctions and the eigenfunctions are orthogonal to each other. This will lead to unitarisation (saturation) corrections which would substantially affect the properties of the ground state. We know, for example from the analysis of HERA data in terms of the Golec-Wuesthoff or BGK model [19, 21], that the saturation corrections damps the effective exponent of the gluon density, $\lambda \approx 0.3$ at $Q^2 \approx 50$ GeV$^2$, to the value which is compatible with the non-perturbative pomeron state, $\lambda \approx 0.1$, at low $Q^2 \approx 0.5$ GeV$^2$ . In our case, the unitarisation corrections could also damp [5] the $\omega$ value of our hypothetical ground state, $\omega_0 \approx 0.3$, to a value compatible with the soft pomeron.

[4] Taking as example the b=10 GeV$^{-2}$ fit, the $t_c$ values of the first five eigenstates are $t_c(1) = 10.332$, $t_c(2) = 18.838$, $t_c(3) = 27.429$, $t_c(4) = 36,306$, which correspond to the characteristic momenta of $k_c(1) \approx 50$ GeV, $k_c(2) \approx 3,3$ TeV, $k_c(3) \approx 260$ TeV, $k_c(4) \approx 21000$ TeV. Taking as $\Delta t = t_c(2) - t_c(1) \approx 8.5$ we obtain from $t_c(0) = t_c(1) - \Delta t$ a value $k_c \approx 700$ MeV. Other values of $k_c(0)$ can be obtained by noting that the increment $\Delta t$ varies slightly with increasing $n$.

[5] Note that the gluon density (4.2) can be unitarised, by eikonalization, in a similar way as the gluon density in [21] or [22].

Furthermore, we expect that this hypothetical, highly unitarised, ground state should have a $k$ distribution which is quickly falling for $k > k_c$. Therefore, its overlap with the photon form factor would also be quickly diminishing with $Q^2$ and so its contribution would be small at larger $Q^2$. Indeed, the $Q^2$ dependence of the fit quality suggests that such a state could be present, see below.

## 4.6 $Q^2$ dependence

In Table 4 we show the AB-Fit results for different $Q^2$ regions, $Q^2 > 4,\ 6$ and 9 GeV$^2$, for $b = 10$ GeV$^{-2}$ as an example. The fits with $b = 20$ GeV$^2$ and/or the $ABC$ fits show very similar results. The fit with $Q^2 > 4$ GeV$^2$ of Table 4 has a substantially lower quality than

| $Q^2$ cut (GeV$^2$) | 4 | 6 | 9 |
|---|---|---|---|
| $A$ | 0.51852 | 0.51844 | 0.51818 |
| $B$ | 1.58847 | 1.58697 | 1.58356 |
| $\eta_{neg}$ | -0.0911 | -0.0911 | -0.0911 |
| $N_p$ | 59 | 51 | 37 |
| $\chi^2$ | 68.5 | 33.9 | 17.4 |
| $\chi^2/N_{df}$ | 1.25 | 0.72 | 0,52 |

Table 4: Results of the AB-Fit with $x < 0.001$ and $b = 10$ GeV$^{-2}$.

the $Q^2 > 6$ GeV$^2$ one. This may be due to the presence of saturation effects, although the worsening of the fit quality seems to be large as compared to the effects discussed e.g. in ref. [10]. The sizeable improvement of the fit quality for $Q^2 > 9$ GeV$^2$ cannot be, however, attributed to any kind of saturation effects, because the $Q^2$ cut is so high. Therefore, it is possible that the worsening of the fit quality with decreasing $Q^2$ cut, is due to the presence of our hypothetical ground state discussed above.

## 4.7 Extrapolation to very low $x$

In Fig. 15 we show the extrapolation of the $AB$ fit to very low $x$ values, which can be possibly achieved in some future $ep$ collider like VHEeP or LHeC. We see that at very large energies the increase of $F_2$ shows similar slopes at different $Q^2$ values, unlike at HERA. This is due to the dominance of the leading trajectory at very low $x$ values.

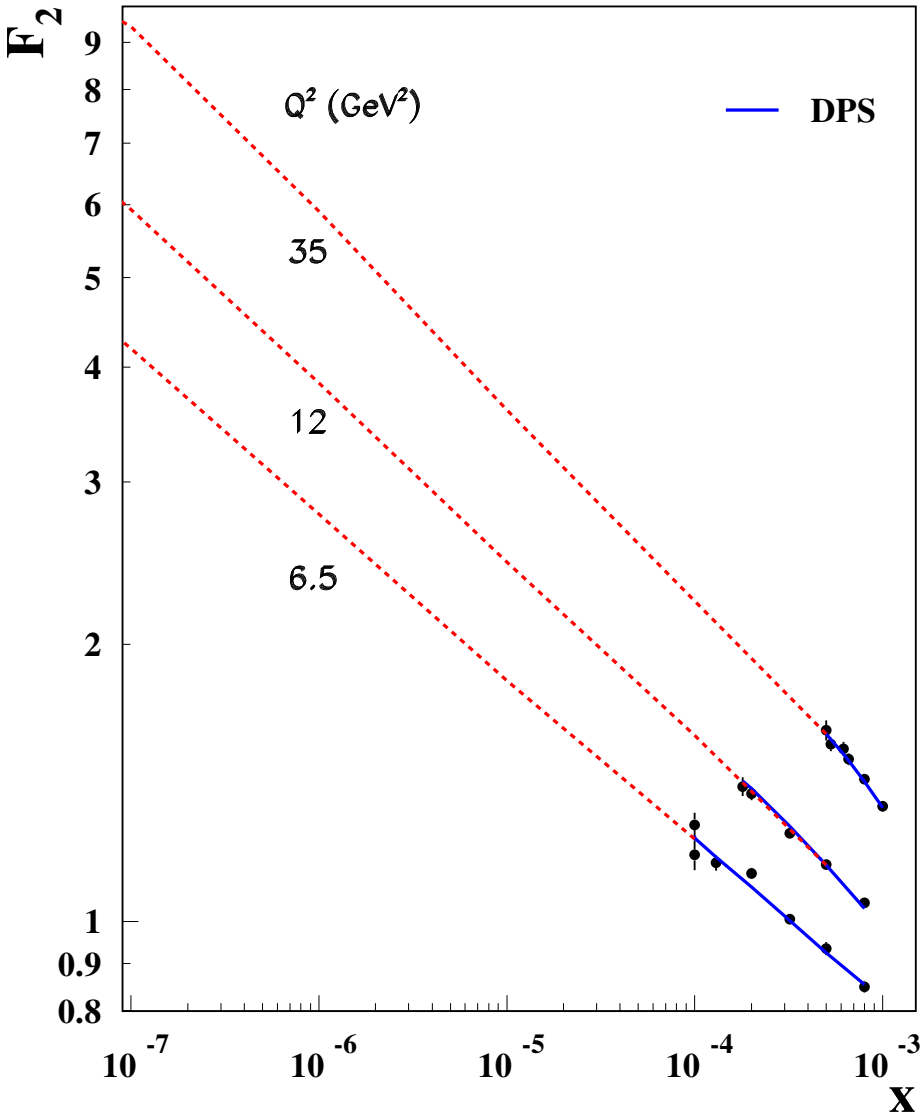


Figure 15: Extrapolation of the AB fit results to very low $x$

# 5 Conclusions and Outlook

We have shown here that there exists a boundary condition, which leads to a precise description of HERA $F_2$ data, for $x < 0.001$. We formulated it in terms of a relation between the eigenvalues, $\omega_n$, and the principal eigenfunction number, $n$. It has a simple form $\omega_n = A/(B+n)$ or $\omega_n = A/(B+n)+C$, called here $AB$ or $ABC$ respectively. Both relations are well motivated in BFKL for larger $n$. The $\omega - n$ relation determines, within the BFKL Green Function solution, the values of the phases of the eigenfunctions, $\eta_n$, close to the non-perturbative region of small $k \sim \Lambda_{\rm QCD}$. The fits using both relations give an excellent description of data with equivalent $\chi^2$ values.

The fits lead to an unexpected result that the first eigenfunction decouples or nearly decouples. This means that the overlaps of the first eigenfunction with the proton form factor are very small or even compatible with zero due to the fact that the first eigenfunction has a transition region from negative to positive values, i.e. a node. Therefore, the first eigenfunction chosen by the fit cannot be a ground state, as is proven in Appendix B. The discussion in the text suggests, as a consequence, the existence of a multiply interacting ground state which could be identified with the soft, saturated, pomeron. The contributions of such a state would quickly disappear as $Q^2$ increases. We may try to learn more about it in our forthcoming paper by focusing the investigation on the region closer to $\Lambda_{QCD}$, by varying $k_0$ and, last but not least, using the full information about the errors of HERA data [12].

The present BFKL fits to HERA data predict that in the very low $x$ region, $x << 10^{-4}$, $F_2$ should grow with a slope $\lambda$ which is close to the eigenvalue of the second eigenfunction and which is $Q^2$ independent. This prediction could be easily verified on some future $ep$ collider, like VHEeP [26] or LHeC [25].

# 6 Appendix A

We rephrase here the original derivation of the BFKL resummation given in ref. [7]. It is convenient to write

$$\chi_0(\nu) \equiv \chi(0,\nu)$$

where

$$\chi(a,\nu) \equiv 2\Psi(1) - \Psi\left(\frac{1}{2}+a+i\nu\right) - \Psi\left(\frac{1}{2}+a-i\nu\right) \tag{6.1}$$

and

$$\dot{\chi}(a,\nu) \equiv \frac{d}{da}\chi(a,\nu) = -\Psi'\left(\frac{1}{2}+a+i\nu\right) - \Psi'\left(\frac{1}{2}+a-i\nu\right) \tag{6.2}$$

If $a$ is small then up to order $a$ we have

$$\chi(a,\nu) = \chi(0,\nu) + a\dot{\chi}(0,\nu) + \mathcal{O}\left(a^2\right), \tag{6.3}$$

We may write $\chi_1(\nu)$ (defining a quantity $\chi_1^{reg}(\nu)$ ) as

$$\chi_1(\nu) \equiv -A\chi(0,\nu) + B\dot{\chi}(0,\nu) + \frac{1}{2}\chi(0,\nu)\dot{\chi}(0,\nu) + \chi_1^{reg}(\nu) \tag{6.4}$$

By a suitable choice of the constants $A$ and $B$, we can arrange for $\chi_1^{reg}(\nu)$ to be free of singularities as $\nu \to, \pm\frac{i}{2}$

In this limit we have

$$\chi(0,\nu) \overset{\nu\to\pm i/2}{\longrightarrow} \frac{1}{\left(\frac{1}{2}\pm i\nu\right)} + \mathcal{O}\left(\frac{1}{2}\pm i\nu\right) \tag{6.5}$$

and

$$\dot{\chi}(0,\nu) \overset{\nu\to\pm i/2}{\longrightarrow} -\frac{1}{\left(\frac{1}{2}\pm i\nu\right)^2} + \frac{\pi^2}{3} + \mathcal{O}\left(\frac{1}{2}\pm i\nu\right) \tag{6.6}$$

So that

$$\chi_1(\nu) \overset{\nu\to\pm i/2}{\longrightarrow} -\frac{1}{2\left(\frac{1}{2}\pm i\nu\right)^3} - \frac{B}{\left(\frac{1}{2}\pm i\nu\right)^2} - \left(A+\frac{\pi^2}{6}\right)\frac{1}{\left(\frac{1}{2}\pm i\nu\right)} \tag{6.7}$$

Therefore the constants $A$ and $B$ are selected to match the single and double poles respectively of the function $\chi_1(\nu)$ and in that way $\chi_1^{reg}$ is free from such singularities.

Salam points out that the correction due to $\chi_1^{reg}$ is genuinely negligible and the entire large correction to the characteristic function come from the terms which are singular as $\nu \to \pm i/2$.

Now let us consider another function $\tilde{\omega}(\nu)$ which is defined as the solution to the transcendental (implicit) equation

$$\tilde{\omega}(\nu) \equiv \bar{\alpha_s}(1-\bar{\alpha_s}A)\chi\left(\frac{\tilde{\omega}}{2}+\bar{\alpha_s}B,\nu\right)+\bar{\alpha_s}^2\chi_1^{reg}(\nu) \tag{6.8}$$

Solving to leading order in $\bar{\alpha_s}$ we have

$$\tilde{\omega} = \bar{\alpha_s}\chi(0,\nu)+\mathcal{O}\left(\bar{\alpha_s}^2\right). \tag{6.9}$$

Expanding $\tilde{\omega}(\nu)$ up to order $\bar{\alpha_s}^2$, and using (6.3) we obtain

$$\begin{aligned}\tilde{\omega}(\nu) &= \bar{\alpha_s}(\chi(0,\nu) + \bar{\alpha_s}^2\left[-A\chi(0,\nu)+B\dot{\chi}(0,\nu)+\frac{1}{2}\chi(0,\nu)\dot{\chi}(0,\nu)+\chi_1^{reg}(\nu)\right]+\mathcal{O}\left(\bar{\alpha_s}^3\right)\\ &= \bar{\alpha_s}(\chi_0(\nu)+\bar{\alpha_s}^2\chi_1(\nu)+\mathcal{O}\left(\bar{\alpha_s}^3\right)\end{aligned} \tag{6.10}$$

Thus we see that up to order $\bar{\alpha_s}^2$, the quantities $\omega(\nu)$ and $\tilde{\omega}(\nu)$ are identical so that up to that accuracy we may replace the usual perturbative expression given in (3.1) by $\tilde{\omega}(\nu)$.

On the other hand, the quantity $\tilde{\omega}(\nu)$ *does not contain any singularities* as $\nu \to \pm\frac{i}{2}$. The singularities we see in eq(6.10) are *only present as a result of an expansion.* They are therefore an artifact of this expansion and are not present for the entire function. Since it is these singular terms that give rise to the large NLO corrections found in $\chi_1(\nu)$ we may consider the quantity $\tilde{\omega}(\nu)$ to be the expression in which all of these large corrections have been resummed.

For the case of the cubic pole, this has been established exactly, since we know what the origin of the triple pole is. Salam explains that this arises from a mismatch between the "rapidity", $Y$, of the forward gluon-gluon scattering amplitude used in the BFKL approach

$$Y = \ln\left(\frac{s}{kk'}\right)$$

For the resummation of the double and single poles, this is not known uniquely and there are several resummation schemes, of which the one described here is one. What they have in common is that they all resum all the collinear singularities (i.e. all poles as $\nu \to \pm\frac{i}{2}$ and they are all equivalent to the ordinary pertubative expansion for $\omega$ up to order $\bar{\alpha_s}^2$. They, of course, differ, in the terms proportional to $\bar{\alpha_s}^3$ and higher - but we have no reason to select one of these schemes above another in the absence of the NNLO calculation of the characteristic function. Scheme 3, which is the scheme considered here is the most convenient for our purposes.

# 7 Appendix B

## Absence of nodes in the wave function of a ground state

One can define the kinetic energy, $\widetilde{T}[\psi]$, as

$$\widetilde{T}[\psi] = -\frac{1}{2m}\int_{-\infty}^{\infty}\psi(x)\,\psi''(x)dx. \tag{7.1}$$

Integrating by parts we obtain

$$T[\psi] = \frac{1}{2m}\int_{-\infty}^{\infty}((\psi'(x))^2dx, \tag{7.2}$$

provided the wave function $\psi(x)$ is continuous and has continuous first derivatives. (The transition from (7.1) to (7.2) is not valid for the continuous wave functions which do not have a fully continuous first derivatives, like e.g. $\psi(x) \sim \alpha|x|$ or $\psi(x) \sim \exp(-\alpha|x|)$.) In the following, we prefer to use for kinetic energy the expression (7.2) since, in contrast to (7.1), it is always positive.

Let us first consider the case of the one-dimensional Schrödinger equation and define the total energy as a functional

$$E[\psi] = T[\psi] + V[\psi] = \frac{1}{2m}\int_{-\infty}^{\infty}(\psi'(x))^2dx + \int_{-\infty}^{\infty}(\psi(x))^2V(x)\,dx\,. \tag{7.3}$$

In the case of a ground state of energy $E_0$, the functional $E[\psi]$ takes the minimal value calculated on all possible normalized wave functions

$$E_0 = \min_{\psi}\frac{E(\psi)}{||\psi||^2}\,,\ ||\psi||^2 \equiv \int_{-\infty}^{\infty}(\psi(x))^2\,dx\,. \tag{7.4}$$

Let us assume, that the $\psi$-function changes its sign, for example, $\psi(x)|_{x\to 0} \sim x$, and prove, that there is a positive function $\chi(x)$ with $\chi(0) \neq 0$, which has a smaller energy $E$. It would mean, that the wave function $\psi$ with a node at $x = 0$ cannot be the wave function of the ground state.

We are choosing the trial wave function $\chi(x)$ in the form

$$\chi(x)|_{|x|>\epsilon} \equiv |\psi(x)|\,,\ \chi(x)|_{|x|<\epsilon} \equiv \frac{|\psi'(0)|}{2|\epsilon|}\left(x^2+\epsilon^2\right)\,,\ \psi(x)|_{|x|<\epsilon} \approx |\psi'(0)|\,x\,, \tag{7.5}$$

where $\epsilon \to 0$. Note, that $\chi(x)$ is a continuous function having also continuous derivatives at $x = \pm\epsilon$. One can neglect small corrections $\sim \epsilon^3$ to the normalisation integral and to the potential energy $V(\chi)$. The main contribution to $\delta E(\chi)$ is obtained from the kinetic energy

$$\delta E = T(\chi) - T(\psi) = \frac{1}{2m}\int_{-\epsilon}^{\epsilon}(\psi'(0))^2\left(x^2/\epsilon^2 - 1\right)dx = -\frac{2(\psi'(0))^2\epsilon}{3m}\,. \tag{7.6}$$

Because $\delta E < 0$ we conclude that, in case of the Schrödinger equation, the ground state wave function cannot have nodes.

Let us turn now to the BFKL equation with the running coupling constant. In the leading logarithmic approximation we have

$$-\omega\, f = H_{BFKL}\, f\,, \tag{7.7}$$

with

$$H_{BFKL} = \sqrt{\alpha_s(t)}\,\left(\Psi\left(\frac{1}{2}+i\nu\right)+\Psi\left(\frac{1}{2}-i\nu\right)-2\Psi\left(1\right)\right)\,\sqrt{\alpha_s(t)}\,, \tag{7.8}$$

where

$$\alpha_s(t) = \frac{1}{\bar\beta_0 t}\,,\ t = \ln\frac{|k_\perp|^2}{\Lambda^2_{QCD}}\,. \tag{7.9}$$

Here $E = -\omega$ plays the role of the total energy in the Schrödinger equation. The operator $\nu$ denotes the momentum canonically conjugated to the coordinate $t$,

$$[\nu, t] = i\,. \tag{7.10}$$

As usual in QCD, one can use the perturbative hamiltonian $H$ for large $t > t_0 > 0$ only. For $t < t_0$ it should be substituted by an hermitian non-perturbative hamiltonian $\widetilde{H}$ and the corresponding wave functions and their derivatives are matched at $t = t_0$.

We prove now that the ground state wave function $f_0$, with energy $E_0$, cannot have a node at $t = t_1 > t_0$. For this purpose, as in the above case of the usual quantum mechanics, we use a simple trial function $\chi(t)$, which is different from $|f(t)|$ (with $f(t_1) = 0$) only in the small region $\sim \epsilon$ around $t = t_1$

$$\chi(t)|_{|t-t_1|<\epsilon} \equiv \frac{|f'(t_1)|}{2|\epsilon|}\,\left((t-t_1)^2+\epsilon^2\right)\,,\ f(t)|_{|t-t_1|<\epsilon} \approx |f'(t_1)|(t-t_1)\,,\ \epsilon \ll 1\,. \tag{7.11}$$

Note, that for the BFKL hamiltonian, which has a non-linear dependence from $\nu^2$, it would be natural to introduce a trial function $\chi$ with continuous higher derivatives in the points $t - t_1 = \pm\epsilon$. But in the correction to the total energy, expressed in terms of the functional

$$E = \int dt\, f(t)\, H\, f(t)\,,\ ||f|| = 1 \tag{7.12}$$

with the substitution $f(t) \to |f(t)| \to \chi(t)$, the contribution from the region $|t - t_1| > \epsilon$ will cancel. In the region $|t - t_1| < \epsilon$, the higher derivatives of the BFKL hamiltonian $H$, acting on the simple polynomial functions $\chi(t)$ and $f(t)$, should be neglected. Note that this corresponds to the diffusion approximation, because only terms proportional to $\nu^2$, in the expansion of the hamiltonian $H$, should be taken into account.

As above, corrections to the normalisation condition and to the running coupling factors $\sqrt{\alpha_s(t)}$ are small. Thus, the main correction to the total energy of the trial function can be written as

$$\delta E = \int_{t_1-\epsilon}^{t_1+\epsilon} \alpha_s(t_1)\, 14\zeta(3)\,(\chi'^2(t) - f'^2(t))dt = -14\zeta(3)\,\alpha_s(t_1)\, f'^2(t_1)\frac{4\epsilon}{3}\,, \tag{7.13}$$

when $\epsilon \to 0$. Because this correction is negative. we conclude that the ground state wave function for the BFKL pomeron cannot have nodes.

# Acknowlegments

We are grateful to Jochen Bartels, Agustin Sabio-Vera, Anna Stasto and Gia Dvali for useful conversations. One of us (LL) would like to thank the State University of St. Petersburg for the grant SPSU 11.38.223.2015 and the grant RFBI 16-02-01143 for support. One of us (DAR) wishes to thank the Leverhulme Trust for an Emeritus Fellowship.

# References

[1] L. N. Lipatov, H. Kowalski, and D. A. Ross, Eur.Phys.J. **C74** (2014) 2919

[2] H. Kowalski, L.N. Lipatov, D. A. Ross, Eur. Phys. J **C76** (2016) 3

[3] L. N. Lipatov, Sov. Phys. JETP **63** (1986) 904.

[4] H. Kowalski, L.N. Lipatov, D. A. Ross, and G. Watt Eur. Phys. J **C70** (2010) 983; Nucl. Phys **A854** (2011) 45

[5] H. Kowalski, L.N. Lipatov,and D. A. Ross, Phys. Part. Nucl. **44** (2013) 547

[6] J. Kwiecinski, A. D. Martin and A. M. Stasto, Phys. Rev. D **56** (1997) 3991.

[7] G. P. Salam, JHEP **9807** (1998) 019.

[8] H. Abramowicz *et al.* [H1 and ZEUS Collaborations], Eur. Phys. J. **C75** (2015) nb.12.

[9] A. Caldwell, "Behavior of $\sigma^{\gamma p}$ at Large Coherence Lengths", axXiv:**0802.0769** (2008)

[10] A. Luszczak and H. Kowalski, Phys.Rev. **D95** (2017) no.1, 014030

[11] A. Caldwell, D. Kollar, K. Krninger, BAT - The Bayesian Analysis Toolkit, Comput. Phys. Commun. 180 (2009) 2197-2209 (ScienceDirect) [arXiv:0808.2552]

[12] S. Alekhin et al., Eur.Phys.J. **C75** (2015) no.7, 304

[13] V.N. Gribov and L.N. Lipatov, Sov. Nucl. Phys. **15** (1972) 438
G. Altarelli and G. Parisi, Nucl. Phys. **B126** (1977) 298
Yu. L. Dokshitzer, Sov. Phys. JETP **46** (1977) 46

[14] I. I. Balitsky and L. N. Lipatov, Sov. J. Nucl. Phys. **28** (1978) 822; E. A. Kuraev, L. N. Lipatov and V. S. Fadin, Sov. Phys. JETP **44** (1976) 443; V. S. Fadin, E. A. Kuraev and L. N. Lipatov, Phys. Lett. B **60** (1975) 50.

[15] V.N. Gribov, ZhETF 53, (1967) 654.

[16] L.V. Gribov, E.M. Levin, M.G. Ryskin, **Phys.Rept.** 100 (1983) 1-150

[17] L. McLerran, R. Venugopalan, Phys.Rev. **D49** (1994) 2233; **D49** (1994) 3352; **D50** (1994) 2225.

[18] A.H. Mueller, D.N. Triantafyllopoulos, Nucl.Phys. **B640** (2002) 331.

[19] K. Golec-Biernat, M. Wuesthoff, Phys. Rev. **D59**, 014017 (1999); Phys. Rev. **D60**, 114023 (1999).

[20] S. Munier, A. M. Staśto and A. H. Mueller, Nucl. Phys. B **603** (2001) 427.

[21] J. Bartels, K. Golec-Biernat and H. Kowalski, Phys. Rev. D **66** (2002) 014001.

[22] H. Kowalski and D. Teaney, Phys. Rev. **D68** (2003) 114005.

[23] H. Kowalski, L. Motyka and G. Watt, Phys. Rev. **D74** (2006) 074016.

[24] Yu.V. Kovchegov, Phys. Rev. **D60** (1999) 034008; **D61** (2000) 074018.

[25] A Large Hadron Electron Collider at CERN: Report on the Physics and Design Concepts for Machine and Detector, arXiv:**1206.2913** (2012)

[26] A. Caldwell and M. Wing , "VHEeP: A very high energy electronproton collider based on proton-driven plasma wakefield acceleration", axXiv:**1509.00235** (2015)